Angular and Proton Number Dependece of the Rutherford Cross Section and Energy, along with the Thickness of Gold and Carbon

Josefine Bjørndal Robl, Lukas Martin Wick, Malthe Fiil Andersen, and Thomas Hansen

Department of Physics and Astronomy, Aarhus University
Course: Experimental Physics 3
Experimental exercise 4
(Dated: October 22, 2019)

This paper aims to determine the angular and proton number distribution (the latter denoted Z-dependence) of the Rutherford cross section for Rutherford scattering of $^1\mathrm{H}^+$ on gold, along with the thickness of gold and carbon. By scattering $^1\mathrm{H}^+$ ions on a target of two layers (gold and carbon) in front of each other and detecting the amount of scattered events for specific angles the angular dependence of the Rutherford cross section is found to follow the expected expression (equation (9)) quite nicely, though some fluctuations being larger than the uncertainties due to the difficulty of fitting the blended gold and carbon peaks for the small angles. The angular dependency of the energy – for gold and carbon respectively – when considering the stopping power is found to be dependent of the kinematic factor and the stopping power, and the energies of the peaks seems to follow the expected energies, but is slightly higher than expected partially due to the calibration not taking the stopping power into account.

The Z-dependency of the Rutherford cross section was found in the same way as the angular dependency, just with various different targets instead of only gold on carbon, along measuring at a specific angle. The Z-dependency was found to be $Z^{1.8(5)}$, which is almost the expected Z^2, and the deviation is expected to be due to the lack of measurements for $Z > 13$, thus also enlarging the uncertainties.

For measurements of the thickness of gold and carbon, the scattered events of $^1\mathrm{H}^+$ on the two gold and carbon samples are found and normalized with the counts from the Faraday cup, and the found thicknesses were

$$t_{\mathrm{Au},1} = 0.05(124) \times 10^3 \,\text{Å}, \quad t_{\mathrm{C},1} = 1.40(1) \times 10^3 \,\text{Å}, \quad \text{and}$$
$$t_{\mathrm{Au},2} = -0.05(626) \times 10^3 \,\text{Å}, \quad t_{\mathrm{C},2} = 0.270(2) \times 10^3 \,\text{Å},$$

for sample 1 and sample 2 respectively. Both samples consists of a layer of gold with a thickness $t_{\mathrm{Au,theo}} = 0.025 \times 10^3 \,\text{Å}$ in front of a carbon layer of either thickness $t_{\mathrm{C,1,theo}} = 1.500 \times 10^3 \,\text{Å}$ (sample 1) or $t_{\mathrm{C,2,theo}} = 0.250 \times 10^3 \,\text{Å}$ (sample 2). For both carbon layers the experimental thicknesses and the expected are fairly consistent, but the experimental thicknesses of gold are not to be trusted due to their uncertainties being several magnitudes larger than their value, which may be due to the lack of measurements for either sample or the fact that the calibration, which was used to fit away the background radiation, was done using sample 2 with the assumption of the thickness of gold to be zero.

I. INTRODUCTION

The elastic scattering of energetic ions called Rutherford scattering was described in 1911 by Ernest Rutherford and led to the development of the plane-tary Rutherford model of the atom and later to the Bohr atomic model. Rutherford scattering is primarily used to determine impurities concentrated on or within a few micrometers of the surface of an otherwise pure material, since it can be combined with
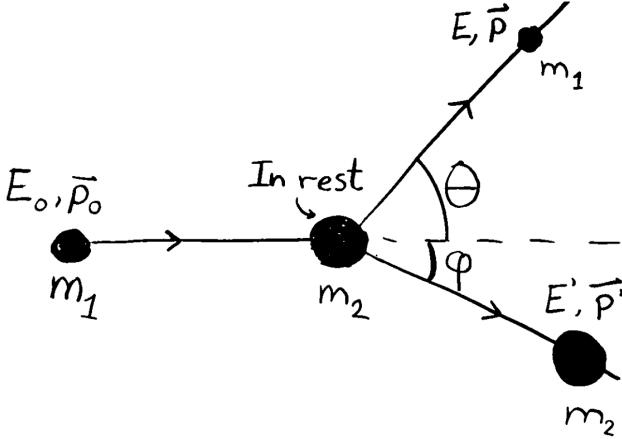
Figure 1: Projectile with energy E_0, momentum $\vec{p_0}$ and mass m_1 scattering upon a target with mass m_2 in rest, resulting in the projectile getting the energy E and momentum $\vec{p}$ and the target to get energy E' and momentum $\vec{p'}$.

channeling [1, 2].

This paper aims to determine the angular and proton number dependence (the latter denoted Z-dependence) of the Rutherford cross section when $^1H^+$ are scattered upon a target nuclei; gold for the angular dependence, and lithium, boron, carbon, fluorine, aluminum, and gold for the Z-dependence. Due to Rutherford scattering being a suitable method for measuring the thickness of targets of high atomic numbers supported on a material with a low atomic number [3], it is in this paper also wanted to examine the thickness of the layers of gold and carbon to see, if the conclusion of [3] can be reproduced.

II. THEORY

Relating the energy of the incident particle (projectile) with the energy of the same particle after the scattering is of great importance for the experiments conducted. A sketch of the scattering can be seen in Figure 1.

By requiring conservation of momentum, one obtains two equations; one for the conservation of momentum parallel to the direction of the projectile and one for the conservation orthogonal to the projectile

direction,

$$p_0 = p\cos(\theta) + p'\cos(\varphi), \quad \text{and} \quad (1)$$
$$0 = p\sin(\theta) + p'\sin(\varphi), \quad (2)$$

where p_0 and p is the momentum of the projectile of mass m_1 before and after the scattering respectively, and p' is the momentum of the scattering target after the scattering. Adding the rearranged and squared versions of equations (1) and (2) we obtain

$$\frac{v}{v_0} = \frac{m_1\cos(\theta) \pm \sqrt{m_2 - m_1\sin(\theta)}}{m_1 + m_2}, \quad (3)$$

where v and v_0 is the speed of the projectile after and before the scattering.

Due to Rutherford scattering being an elastic scattering, conservation of kinetic energy is required, hence squaring equation (3) and inserting, one obtains

$$E = \left(\frac{m_1\cos(\theta) + \sqrt{m_2 - m_1\sin(\theta)}}{m_1 + m_2} \right)^2 E_0 = K^2 E_0, \quad (4)$$

where E_0 is the incident energy of the projectile, E the energy of the projectile after the scattering, and K is the kinematic factor, where the positive solution is chosen due to $m_2 \gg m_1$, thus the negative solution would result in negative energies.

In this derivation the particles have been assumed to classical which is reasonable as with protons (the lightest projectile used) a classical calculation of the velocity gives: $0.03c$.

A. Calibration

For the calibration it is needed to be able to change the magnetic field strength of a magnet due to a change in the mass of particles the magnet shall deflect. The magnet supplies uniform magnetic field perpendicular to the movement of the particles, hence their trajectory in the magnetic field will be part of a circular motion, thus the particle will be subject to the centripetal force

$$F_{cen} = \frac{mv^2}{r}, \quad (5)$$

where m and v is the mass and the speed of the particle respectively and r is the radius of the circular motion. Equating the centripetal force (equation (5))

with the Lorentz-force (with no present electric field), the radius due to the magnetic field is found, and for two particles with different mass to travel down the same path the radii of both trajectories must be equal, so

$$\frac{m_1 v_1}{q_1 B_1} = \frac{m_2 v_2}{q_2 B_2} \,, \qquad (6)$$

hence the strength magnetic field of the first particle as a function of the other particles magnetic field strength

$$B_2 = \frac{m_2 v_2 q_1}{m_1 v_1 q_2} B_1 \,. \qquad (7)$$

By restricting the particles to have the same energy, thus $v_2/v_1 = \sqrt{m_1/m_2}$, and the same charge equation (7) becomes

$$B_2 = \sqrt{\frac{m_2}{m_1}} B_1 \,. \qquad (8)$$

B. Rutherford Cross Section

Rutherford scattering is an elastic scattering occurring when a charged projectile is travelling towards a heavier nucleus, thus being deflected due to the Coulomb interaction.

Three assumptions are needed for the derivation of the cross section [4]: Firstly the projectile and the scattering target are assumed to be point particles. Secondly the mass difference between the projectile and target shall be so large, that the scattering target can be considered infinitely heavy. Lastly we only consider the monopole term of the the electrostatic Coulomb force with the Coulomb potential $V_C = \pm C/r$. From these assumptions we get the Rutherford cross section to be

$$\frac{d\sigma}{d\Omega} = \left(\frac{Z_1 Z_2 e^2}{4 E_i} \right)^2 \frac{1}{\sin^4(\theta/2)} \,. \qquad (9)$$

For an extended nucleus the quantum mechanical derivation is used. It is assumed that the charge distribution is homogeneous, and using Fermi's Golden Rule of perturbation theory for a sufficient weak perturbation along with the first Born approximation, the Rutherford cross section for an extended nucleus is found to be the squared absolute value of the form factor, F, of the nucleus times the Rutherford cross section for a point nucleus (equation (9)) [4].

$$\frac{d\sigma}{d\Omega} = \left(\frac{d\sigma}{d\Omega} \right)_{\text{point nucleus}} |F|^2 \,. \qquad (10)$$
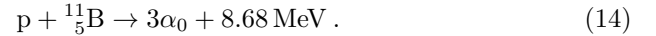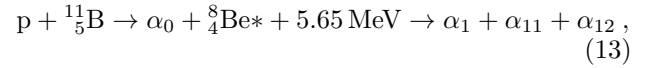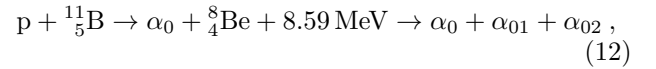
C. Thickness of Targets

When a beam travels through a material, the beam looses energy due to the stopping power of the material, hence the energy loss is:

$$\Delta E = - \int_0^t s(E) \, dt \,, \qquad (11)$$

where $s(E)$ is the stopping power, which is depending on the energy by $s(E) \equiv -\frac{dE}{dt}$, where t is the thickness [5].

D. Proton Incident on Boron

When a photon is incident on boron an aneutronic fusion process happens and produces three alpha particles [6]:

$$p + {}^{11}_5B \rightarrow \alpha_0 + {}^8_4Be + 8.59\,\text{MeV} \rightarrow \alpha_0 + \alpha_{01} + \alpha_{02} \,, \qquad (12)$$

$$p + {}^{11}_5B \rightarrow \alpha_0 + {}^8_4Be* + 5.65\,\text{MeV} \rightarrow \alpha_1 + \alpha_{11} + \alpha_{12} \,, \qquad (13)$$

$$p + {}^{11}_5B \rightarrow 3\alpha_0 + 8.68\,\text{MeV} \,. \qquad (14)$$

The dominant reactions being equations (12) and (12) go through the formation of a ${}^{12}C*$, which decays into an alpha particle and an unbound ${}^8Be$, in its fundamental and first-excited state respectively, which further decays to two alpha particles. Also the direct 3-body reaction, equation (14), is possible, but less likely than the other two.

III. SETUP AND PROCEDURE

Figure 2 is a diagram of the setup used for all the measurements in this experiment can be seen.

First the beam leaves the Van de Graff acelerator, enters aset of deflectorplates (two vertical and one horizontal), used to change the beams trajectory, so it ends up reaching the detector. The magnet has two purposes: Firstly to help chose whether the ${}^1H^+$, ${}^2H^+$
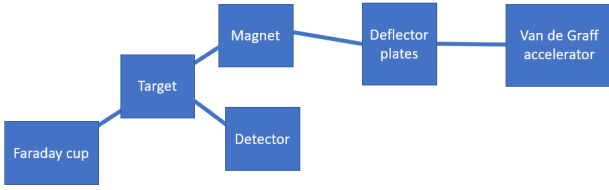
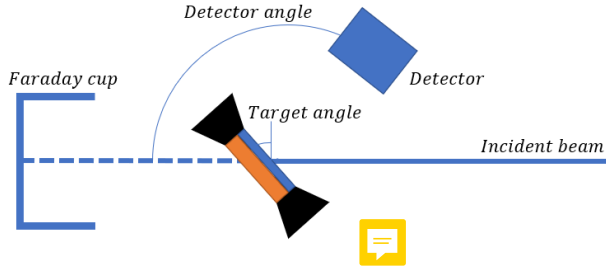*Figure 2: Diagram of the setup used for this experiment*

Figure 3: Diagram of the setup around the target

or the ^{3}H$^+$ ions are to reach the detector (see subsection II A) and secondly to act as the sencond deflector plate.

The section around the target, detector and faraday cup is diagrammed in Figure 3.

A. Calibration

In order to calibrate the setup regarding energy output different hydrogen ions were used, specifically: ^{1}H$^+$, ^{2}H$^+$ and ^{3}H$^+$. The detector is set to 160° and the scattered ions are measured. The different ions are expected to result in different scattering energies as upon impact the ions will break into one, two and three pieces respectively with the same energy.

Thus three points of scattering energy of 160° half of that and a third of it respectively. The expected energy for the ^{1}H$^+$ ion can be caculated theoretically given the energy prior to the collision, see equation (4).

The particular ion one wants to test with can be chosen using the magnet, see subsection II A.

The 160° was chosen as at high angels the energy difference of scattering on fore example gold and carbon differ maximally, and thus it becomes easier to differentiate the different peaks.

No particular measuring time was chosen as the interesting point is the energies and not the count numbers. This means that the time can be chosen such that the peaks are well formed.

Another 3 points can be obtained by changing the incident energy, the measurements were done for all 3 ions for incident energy of 350 keV and 400 keV, giving 6 points in total.

B. Angular Dependence of Differential Cross Section and Energy

The cross section was measured using ^{1}H$^+$ on a target consisting of 25 Å gold placed on a 250 Å carbon sheet. The gold was pointed towards the incident beam. The faraday cup was connected to a counter allowing for measurement of the amount of radiation pasing through the target The measurements were done inn steps of 10° from 160° to 30° excluding the measurements from 100° to 80° due to the fram the target was placed in. One measurement at 105° was also conuducted. The measurements were taken over a 600 seconds period for 160° to 70° excluding the 105° measurement which were taken over 400 seconds. The 60° measurement was done over 350 s, the remaining were done over 300 s.

C. Z_{target}-dependece of the Cross Section

In order to measure the dependence of the cross section of the core charge of the atom (Z) a series of different targets are used, thus varying Z. This leads to varying absorptions of protons in the target. This means that the Faraday cup can not be used to measure the beam flux, see Figure 2.

In order to get around that issue a measurement without a target is taken before and after each actual measurement. If the beam flux is the same in both of them it can be assumed that the beam was constant during the measurements, otherwise it must be assumed that the change is linear.

The measurements themselves then consist of setting the detector to 160°, setting up the right target and then measuring the amount of particles hitting the detector over the relevant time, see section IV. The targets consisted of lithium (Z=3), boron (Z=5), carbon (Z=6), fluorine (Z=9), aluminium (Z=13) and gold (Z=79).

The targets consist of two different materials placed on top of each other. This leads to the decision of using 160° since at large angles the energy difference between the peaks is at its maximum see subsection II B,
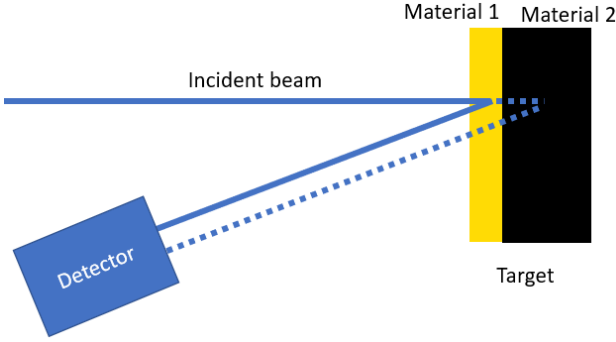
Figure 4: Diagram of the method used to measure the thickness.

D. Thickness of Targets

The target consists of two materials split into two layers, see Figure 4. Depending on which target is in front and which is in the back, the energy peaks will drift a little as a consequence of the stopping power of the materials. Two targets were employed both of which consisted of a thin gold film placed on a thicker carbon sheet.

The stopping power of a material was earlier defined as:

$$s(E) = -\frac{\mathrm{d}E}{\mathrm{d}t}, \tag{15}$$

where t is the thickness of the target and E is the energy of the projectiles. The stopping power depends both on the material and the energy. The function is only known empirically for discrete numerical values.

Firstly, it is important to know that the stopping power is close to constant within intervals of order of the thickness of the layers of the targets (of the order of nano-meters resulting only in small energy changes).

Secondly, it was observed that a high fraction of the incoming projectiles went all the way through the target, while only a few were scattered. That is, the intensity of the beam can be assumed constant[1].

Combined, these two observations allow for the approximation that the observed energy spectrum is symmetric around the energy of a projectile scattered in the *middle* of the material[2]. That is, the spectrum will have a peak around that specific energy. When we do the calculations to find the expected energies, we thus assume that all the projectile particles move into the middle of the relevant material and is scattered back.

One further approximation is used to simplify the calculations greatly; for the incoming projectile the stopping power for the incoming energy is used (thus overestimating the lost energy), and for the outgoing, scattered projectile the outgoing energy for the stopping power is used (which in contrast underestimates the lost energy).

In the following subscript 1 denotes the configuration for gold in front while subscript 2 denotes the opposite. Subscript Au or C denotes scattering on gold or carbon respectively.

Using the assumptions above, we can calculate the measured energy for a scattered particle in gold when gold is placed in front as:

$$E_{1,\mathrm{Au}} = \left(E_0 - s_{\mathrm{Au}}(E_0)\frac{t_{\mathrm{Au}}}{2} \right) K_{\mathrm{Au}}^2 - s_{\mathrm{Au}}(E_{1,\mathrm{Au}})\frac{t_{\mathrm{Au}}}{2\cos(\pi - \theta)} \tag{16}$$

In the same way, the energy for scattering on gold when gold is placed behind is:

$$E_{2,\mathrm{Au}} = \left(E_0 - s_{\mathrm{C}}(E_0)t_{\mathrm{C}} - s_{\mathrm{Au}}(E_0)\frac{t_{\mathrm{Au}}}{2} \right) K_{\mathrm{Au}}^2$$
$$- s_{\mathrm{Au}}(E_{1,\mathrm{Au}})\frac{t_{\mathrm{Au}}}{2\cos(\pi - \theta)}$$
$$- s_{\mathrm{C}}(E_{2,\mathrm{Au}})\frac{t_{\mathrm{C}}}{\cos(\pi - \theta)} \tag{17}$$

Taking the difference between the two gives the change in the energy peak of gold ΔE_{Au} when turning the target. Similarly, the energy change for carbon is cal-

---

[1] In reality the intensity is exponentially decreasing in the target material, but this can be neglected due to the observed facts mentioned.

[2] It is also assumed that the probability of scattering is independent on *how deep* the projectile is in the target.

culated. The two changes can be written as:

$$\Delta E_{\text{Au}} = a \cdot t_{\text{C}} + b \cdot t_{\text{Au}}$$
$$\Delta E_{\text{C}} = c \cdot t_{\text{C}} + d \cdot t_{\text{Au}}, \tag{18}$$

where:

$$a = s_{\text{C}}(E_0)K_{\text{Au}}^2 + \frac{s_{\text{C}}(E_{2,\text{Au}})}{\cos(\pi - \theta)} \tag{19}$$

$$b = \frac{1}{2\cos(\pi - \theta)}\left(s_{\text{Au}}(E_{2,\text{Au}}) - s_{\text{Au}}(E_{1,\text{Au}})\right) \tag{20}$$

$$c = \frac{1}{2\cos(\pi - \theta)}\left(s_{\text{C}}(E_{1,\text{C}}) - s_{\text{C}}(E_{2,\text{C}})\right) \tag{21}$$

$$d = s_{\text{Au}}(E_0)K_{\text{C}}^2 + \frac{s_{\text{Au}}(E_{1,\text{Au}})}{\cos(\pi - \theta)} \tag{22}$$

These are all measurable values. The equations for the thickness of gold and carbon can then be easily solved by using the inverse of a 2-by-2 matrix.

IV. MEASUREMENT PLAN

Here is the measurement plan consisting of the general plan for measurements, but not the overall way in which is was done, nor many of the arguments for the method as both are written in section III.

A. Day 1

As this will be the first time working on this setup it is impossible to plan much ahead regarding the amount of work that can be done, as the practicalities are not yet known to us. So the plan for the first time is to familiarize our selves with the setup and to do some calibration measurements.

The calibration will be done with the detector placed at 160° see section III. This is done in order to make as large a difference between the different peaks from the two materials in the target as possible. The target chosen consist of 25 Å of gold placed on 250 Å of carbon. The choice of target is not too relevant, since the time of measuring can vary according to the observed intensities, given that only the energy is relevant for the energy calibration. Thus the time chosen for the individual measurements are determined by the spectrum, as both the peak associated with carbon and gold need to be clear in order to fit a Gaussian to them, see subsection V A.

B. Day 2

1. prior planning

There are 3 things left that need to be measured:

- The angle dependence of the cross section and energy.

- The thickness of the two targets with gold and carbon

- The Z dependence of the cross section

Of these the angle dependence of the energy and cross section should take by far the most amount of time, so that is what is planned to be done on the second day, as that will hopefully leave plenty of time to do the last two on the final day.

The cross section and energy dependence by angle is plotted theoretically leaving us with the expected result that both drop as the angle increases. This lead to the measurements starting from 160° and decreasing in steps of 10°. The measurements will be done this way as the times chosen, see subsection III B, is discussed prior to entering the lab and measurements for every 10° is the agreed upon minimum for the density of measurements. If any more time is available extra measurements around the gap made by the target frame will be taken, in order to give a more even distribution of the data over the angle spread available.

C. Day 3

As written the thickness of the ´targets with gold and carbon and the Z dependence of the cross section will be measured on day 3. As the magnet needs to stabilize after startup in order to get a steady beam, which is needed to measure the Z dependency of the cross section. This means that the thickness measurements will be done first. The time for the measurements are not important, as only the energy is relevant here, so the spectrum is used to determine the time needed. As the measurements are done with the detector at 160° one of the measurements were done during the calibration, and does not have to be repeated.

The Z dependence of the cross section will be conducted at 160° as the peaks associated with the material measured and any underlying materials (which
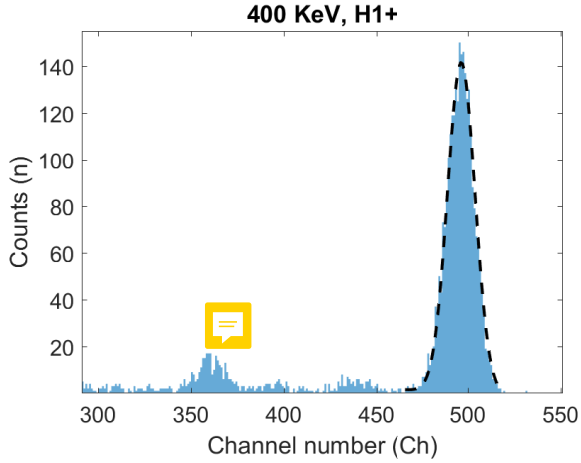
Figure 5: Spectrum of H^+ at $E_{\text{initial}} = 400 keV$ with $\theta = 160°$ together with a Gaussian fit (and linear background)

Figure 6: Fit of calibration with MSE of: 9.3.

are there in some cases but all) needs to distinguishable and the largest distance between them is at large angles. If plenty of time is available a measurement without target is done before and after every measurement, otherwise one will only be conducted before all the measurements and after, and then it could assumed that the change is linear over all the targets. (There ended up being plenty of time).

V. RESULTS

A. Calibration

In order to calibrate the unit of measurement in the program to energy, we exploit the fact that we know the energy of the incoming projectiles (due to the set voltage of acceleration) and the theoretically expected energy at a certain angle (given by equation (4)). We can do this for three different projectiles (single protons, deuterium, and tritium, with $n = 1, 2, 3$ outgoing particles sharing the energy) as well as for two different voltages. This gives six known energies of $E_{\text{final}} = \left(K^2 \cdot E_{\text{initial}} \right) / n$

Of course this calibration assumes the validity of equation (4), which is one of the very points of this paper to prove. That is why we only take the calibration measurements at a given angle. The calibration can at most change the energy values by a constant. But the data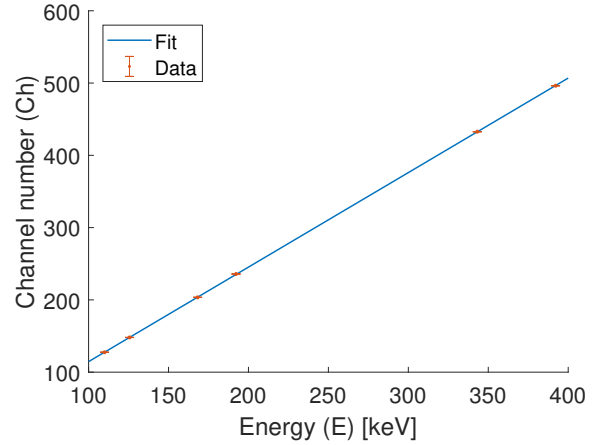 for the angle-dependence of the energy will only be compared to the theoretical curve up to a constant. Consequentially, if the theory is not correct the data and the theory will not artificially agree through the calibration anyway. It is thus practically save to use this method of calibration.

For each energy a measurement was made giving a spectrum as can be seen in Figure 5.

The gold peaks where fitted using a Gaussian with linear background, to find the center. One of these fits can be seen in Figure 5. All of these fits had reasonable MSE (Mean Square Error defined as Chi squared over degrees of freedom of the fit) values of around 1 which given we are only interested in their top points and not their general distribution is fully acceptable. The uncertainty in the center of the peak was found from the fit.

Now the channel number (denoted Ch) can be plotted against energy and a straight line can be fitted through the points as in Figure 6. As the uncertainties are very low a plot of the residuals from the fit is plotted in Figure 7 together with the confidence intervals. The results of the fit is:

$$E = 0.7647(7) \, \text{keV} \cdot Ch + 12.4(2) \, \text{keV}. \qquad (23)$$
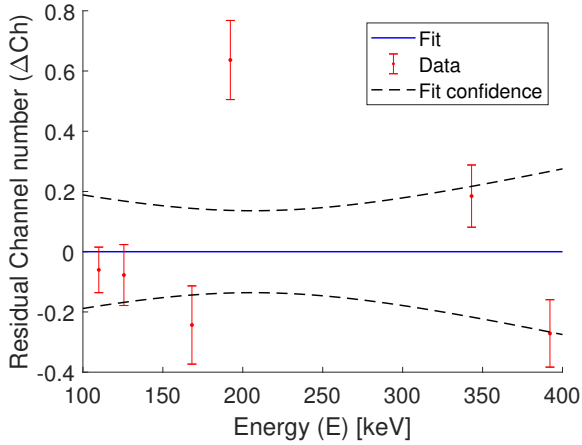
The MSE of this fit was 9.3.

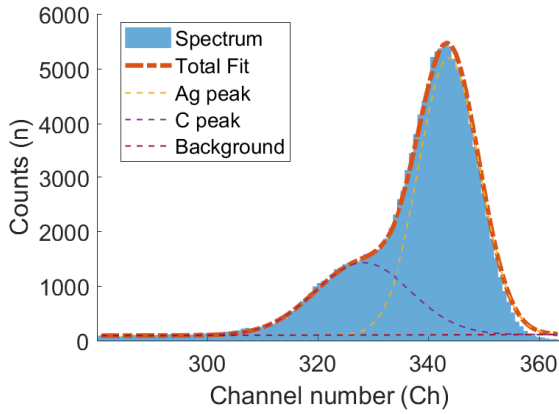Figure 7: *Residual plot of calibration fit in Figure 6.*

Figure 8: *Energy spectrum of sample 2 at 60° with double Gauss and background fitted. As the angle is low the two peaks overlap.*

B. Angular Dependence of Differential Cross Section and Energy

The energy spectrums are fitted to a sum of two[3] Gaussians plus a linear background noise.[4] An example of such a fit can be seen in Figure 8.

This gives the energy of the scattered proton as well as the number of scattered protons. The number of

---

[3] Both the gold and the carbon peaks.

[4] This was done using the peak fitting tool peakfit.m from https://se.mathworks.com/matlabcentral/fileexchange/23611-peakfit-m.
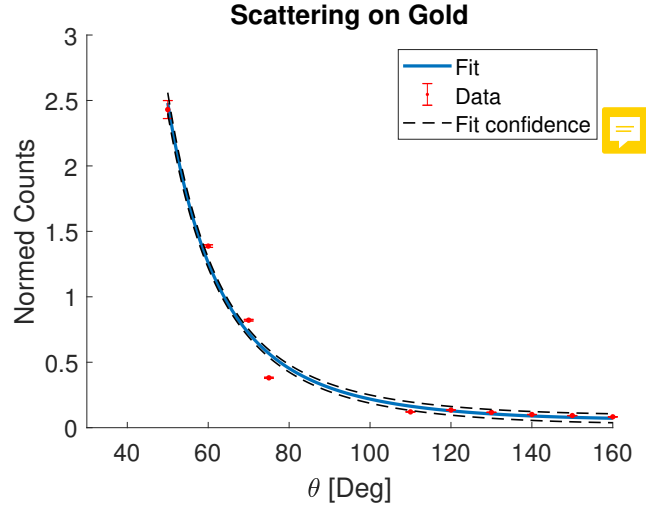

Figure 9: *"Normed" counts (relative to the Faraday-cup) under the gold peak as function of angle, together with the fit and fit confidence.*

scattered protons is normed relative to the counts in the Faraday-cup, since the fraction of counts in the Faraday-cup relative to the total number of incident protons is assumingly constant.

The counts for each angle are compared to the Rutherford differential cross section[5] for gold and carbon up to a fitted coefficient (see Figures 9 to 12). The fitting expression is given as

$$\text{counts} = \beta \frac{1}{\sin^4(\theta/2)}. \tag{24}$$

The β constant is necessary as the intensity of the beam is not precisely known[6].

The energies for each angle compared to the expectations given by kinematic factor and from the the stopping power of the materials (and the given thicknesses $t_C = 250\,\text{Å}$ and $t_{Au} = 25\,\text{Å}$). This can be seen for gold and carbon in Figures 13 and 14. The effects

---

[5] Remember that the Rutherford cross section assumes the nucleus to be a positive point charge. This is in direct contradiction with the plum pudding model of atoms.

[6] With the intensity (and factors like the solid angle of the detector) the exact theoretical values could be calculated. The intensity could in principal be calculated from the counts in the Faraday cup and a calibration with and without the sample, but no such attempt was made
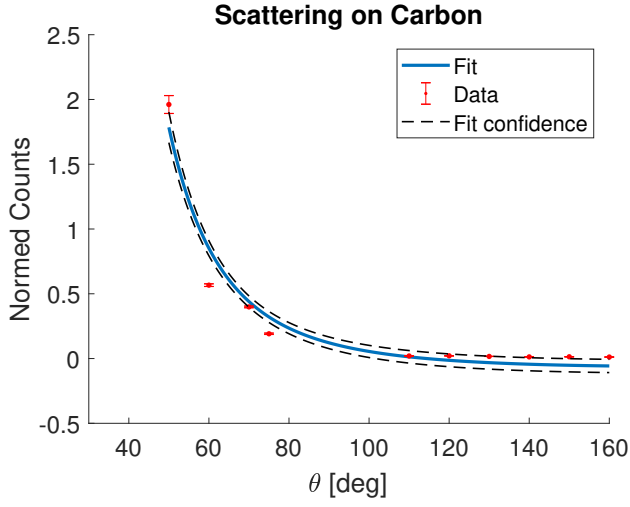
Figure 10: "Normed" counts (relative to the Faraday-cup) under the carbon peak as function of angel, together with fit and fit confidence.
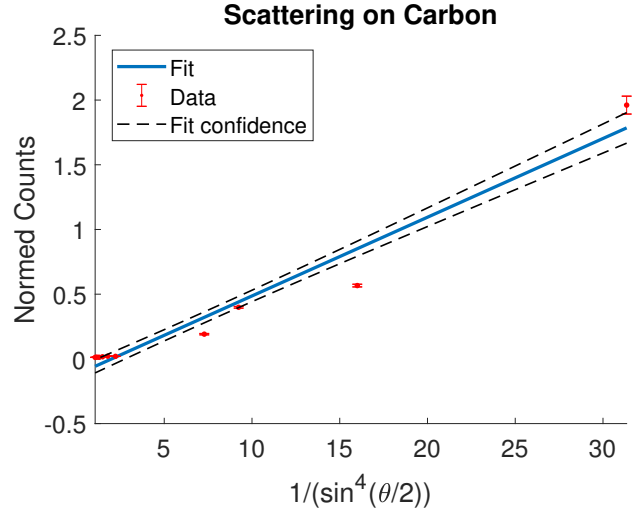

Figure 12: "Normed" counts (relative to the Faraday-cup) under the carbon peak as function of $\frac{1}{\sin^4(\theta/2)}$, together with linear fit.
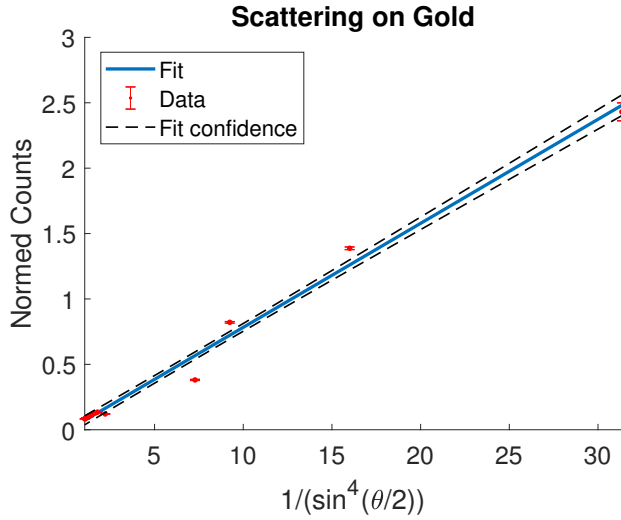

Figure 11: "Normed" counts (relative to the Faraday-cup) under the gold peak as function of $\frac{1}{\sin^4(\theta/2)}$, together with linear fit.

of stopping power is given as

$$
\begin{aligned}
E_{\mathrm{Au}} = \quad & \\
& \text{if } \theta < \pi/2 \\
(E_{in} - T_{\mathrm{Au}}/2S_{\mathrm{Au}})K_{\mathrm{Au}}^2 & - \frac{T_{\mathrm{Au}}/2S_{\mathrm{Au}} + T_C S_C}{|\cos(\theta)|}, \\
& \text{if } \theta > \pi/2 \\
(E_{in} - T_{\mathrm{Au}}/2S_{\mathrm{Au}})K_{\mathrm{Au}}^2 & - \frac{T_{\mathrm{Au}}/2S_{\mathrm{Au}}}{|\cos(\theta)|},
\end{aligned}
$$

and

$$
\begin{aligned}
E_C = \quad & \\
& \text{if } \theta < \pi/2 \\
(E_{in} - T_{\mathrm{Au}}S_{\mathrm{Au}} - T_C/2S_C)K_C^2 & - \frac{T_C/2S_C}{|\cos(\theta)|}, \\
& \text{if } \theta > \pi/2 \\
(E_{in} - T_{\mathrm{Au}}S_{\mathrm{Au}} - T_C/2S_C)K_C^2 & - \frac{T_C/2S_C + T_{\mathrm{Au}}/S_{\mathrm{Au}}}{|\cos(\theta)|},
\end{aligned}
$$

where S_{Au} and S_C are evaluated at the energy calculated at that point in the expression.
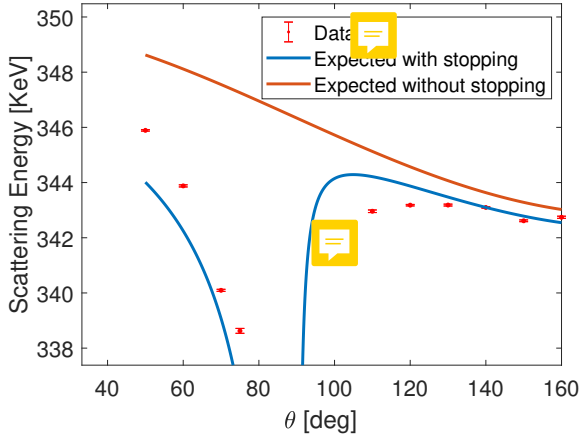
Figure 13: Energy of gold peaks as function of angle together with expected energies with and without stopping power taken into consideration.
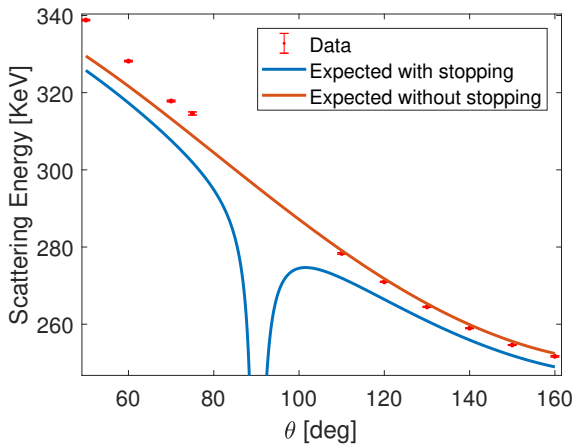

Figure 14: Energy of carbon peaks as function of angle together with expected energies with and without stopping power taken into consideration.

C. Z_{target}-dependence

The Z-dependence of the cross section is predicted to be given as:

$$\frac{d\sigma}{d\Omega} \propto Z^2 \,, \tag{25}$$

see equation (9).

Every measurement contains multiple peaks. The peak associated with scattering on the material of in-
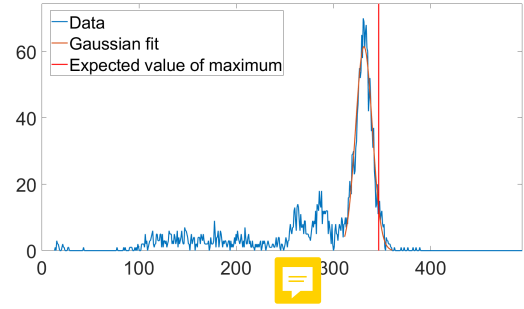

Figure 15: Spectrum of measuring on Aluminium.

terest was determined through calibration and usage of the K-factor, see equation (4).

The peak was then fitted with a gaussian. The fits turned out to have the lowest uncertainty if no background terms were employed, which does not seem completely unreasonable given Figure 15.

The uncertainty on the background radiation were measured by a measurement without target before and after every measurement, see subsection III C. Thus the background was calculated as the average between the two and the uncertainty can then approximated as the difference between the average and one of the two measurements. This is not an ideal way of determining the uncertainty but it is reasonable. As only the dependence of the cross section on Z is relevant some factor which is proportional to the cross section (with the same propotionality factor for all targets) is needed. Here this is called the c-factor:

$$c = \frac{\#_{target}}{\#_{empty} * \rho_S} \tag{26}$$

where $\#$ refers to the amount of particles measured, and target refers to those scattered on the target while empty refers to the empty measurement[7]. ρ_S is the surface density of the target, as the cross section will be proportional to the overall density of the material and the thickness of the target, which varies for for different targets, has to be divided out to get the dependence of Z. Note that thickness times volume density equals surface density.

The uncertainty of $\#_{target}$ was determined using the propagation law and the uncertainty of the fitting parameters.

---

[7]The empty and target measurements were not taken over the same time, but since that should only add a scaling constant between the two, it is not of much importance.
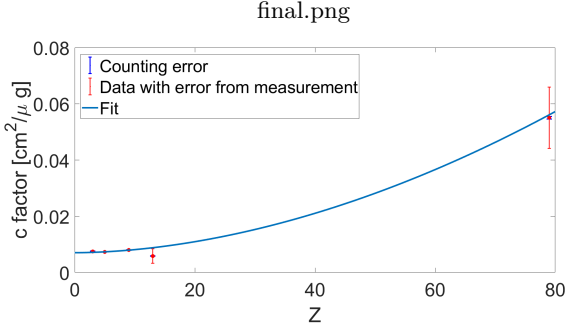
final.png

Figure 16: figure of the fit and data of the Z dependence of the cross section (c factor). The uncertainties on the c-factor was determined using both the calculated uncertainty from the empty measurements see subsection V C.

The uncertainties on the *c*-factor was calculated using the propagation law, using both counting uncertainties and the uncertainties calculated from the empty measurements.

The fit function used was:

$$c = a(1) * Z^{a(2)} + a(3) \tag{27}$$

Where $a(1)$ is included to scale the axis correspondingly and $a(3)$ is to counter background. The exponent turned out to be: 1.8 ± 0.5.

D. Thickness of Targets

Figures 17 and 18 show the energy spectra of the two samples before and after turning the target. This illustrates the drift of the peaks which is used to find the thickness of the targets. The peaks are fitted using a Gaussian with linear background, from which ΔE_{Au} and ΔE_{C} can be calculated for each sample.

Solving equation (18) gives

$$t_{\mathrm{Au}} = 0.05(124) \times 10^3 \,\text{Å}, \quad \text{and}$$
$$t_{\mathrm{C}} = 1.40(1) \times 10^3 \,\text{Å} \tag{28}$$

for the first target (the target with the thickest carbon layer). For the target with thin carbon we get

$$t_{\mathrm{Au}} = -0.05(626) \times 10^3 \,\text{Å}, \quad \text{and}$$
$$t_{\mathrm{C}} = 0.270(2) \times 10^3 \,\text{Å}. \tag{29}$$

Figure 17: Spectrum of sample 1 at $180°$ (pos 2 (Gold in front)) and $0°$ (pos 2 (Carbon in front)). At $160°$ and $350keV$. The Gauss fitted peaks are marked.
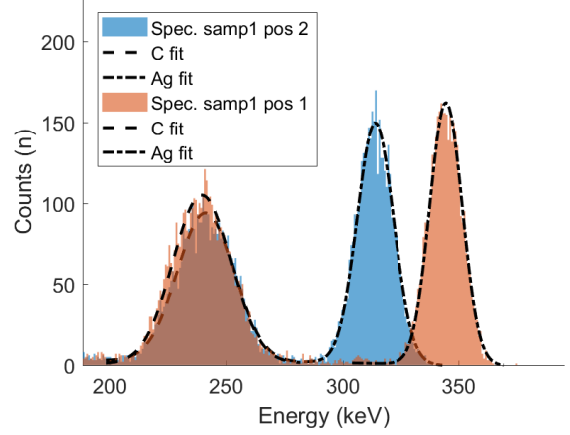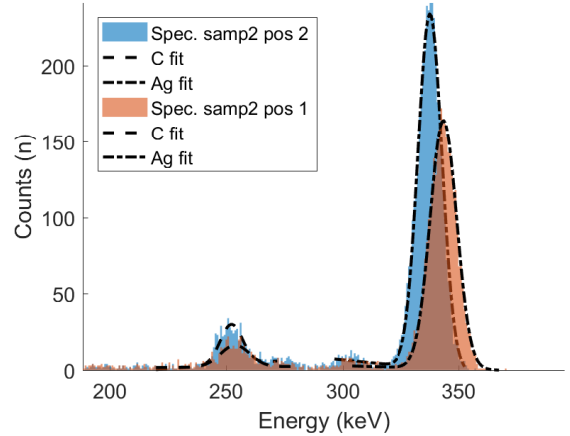

Figure 18: Spectrum of sample 2 at $180°$ (pos 2 (Gold in front)) and $0°$ (pos 2 (Carbon in front)). At $160°$ and $350keV$. The Gauss fitted peaks are marked.

VI. DISCUSSION

A. Angular Dependence of Differential Cross Section and Energy

The found differential cross section and the expected are in close agreement as can be seen in Figures 11 and 12, however with some fluctuations which are quite a bit larger than the uncertainties. One reason is the difficulty we had fitting the overlapping

Gaussian peaks, giving high uncertainty in the results for low angles. The calculated uncertainty also seems rather low and has probably been underestimated. Another, probably way smaller factor is the assumption of a point like target. The shape of the target will introduce a relevant form factor, see equation (10), which is out of the scope of this report to study. It is worth noticing, however, that even though the form factor will result in possible corrections of the theoretical fit, the data is in no way explainable if the plum-pudding model was correct.

The range of the angles are notably a little low as we were not able to fit the overlapping functions. A plot of the spectra with attempted fits can be seen in Figure 19.

The energies of the peaks can be seen in Figure 13 and Figure 14. The carbon peaks nicely follow the expected energies found using only the kinematic factor for high angles, but there seem to be a systematic error for low angles that makes the found energy higher than expected. The energies are notably higher that what is expected when taking the stopping power into account. This might be a result of the fitting method and the linear background slightly shifting the top point. This could indicate that the peaks in general is fitted closer to each other than they should. Again, it seems the uncertainties are estimated too low.

The gold peaks quite nicely follow the expected energies again with slightly too high energy for most angles. Here the effect of the stopping power is clearly represented by the data. The general increase in energy for the peaks is likely partially due to the calibration not taking the stopping power into account giving too high expected energies, which also leads to higher energies in measurements relying on the calibration. A more sophisticated model for the calibration was however not chosen as it could interfere with the measurements of the thickness of the plates, by using the known values before they are found. In principle the measurements should be made recursively until divergence but for the large uncertainties in the thicknesses (see later section) this was deemed unreasonable.

B. Z_{target}-dependence

The peaks from the individual materials were determined as described in subsection V C.

It can clearly be seen in Figure 15 that the peak isn't lying exactly on top of the peak at hand. This is not entirely unexpected as the beam has to pass through the material to scatter, and thus some energy is lost due to the stopping power of the given material. This is also consistent with the expectation lying at higher energies than the actual peak.

The peaks were not fitted using a background, as they seemed to go to zero without them, and the fits fit the data better without them. The background is instead introduced in the fit to the Z-dependence as the minimal background is very close to zero for all peaks and thus pretty constant. It does have a big impact on the exponent in that as the points should go to zero for Z going to zero, and thus small discrepancies can have big impacts.

The Aluminium peak (Z=13) has significantly larger uncertainty than the surrounding peaks, this is due to a unstable beam during the measurement, the before after count dropped from about 15883 to 6046. This also explains the significantly lower value. It should be noted that it is just barely outside 1 sigma under so it does not seem unreasonable.

The data is mainly around low Z values (≤ 13) so a better measurement could have been achieved had more target with high Z values been available, this would likely also lower the uncertainties. The result is quite reasonable. The expected value of 2 is within half a sigma from the final result (1.8(5)) which seems to verify the prediction.

C.   Thickness of Targets

The measured thickness of the thick carbon-layer agrees with the given value of 1.5×10^3 Å within the uncertainties. The measured thickness for the thin carbon layer differs slightly from the 0.250×10^3 Å - even when considering the uncertainties. Since we are not aware of how or when the "official" measurements were taken nor the uncertainties of the measurements, this is not necessarily a problem. To our knowledge, the value $0.270(2) \times 10^3$ Å might be the most trustworthy[8].

The measurements for the thickness of gold, however, are totally worthless. The estimated uncertainties might be off, but there is no doubt they are several magnitudes higher than the actual value. That is why we also find negative values, which is obviously not correct.

---

[8]When discussing the thickness of gold, we will mention reasons for why our values might be off a bit.
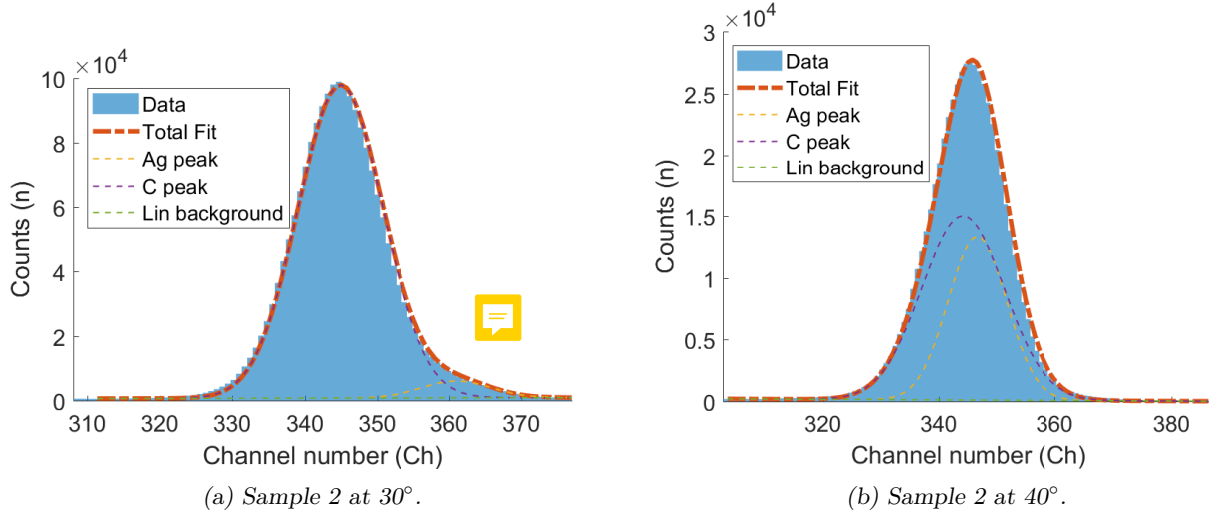
(a) Sample 2 at 30°.

(b) Sample 2 at 40°.

Figure 19: Energy spectrum of samples at respective angels with attempted fit to double Gauss and background.

There are several reasons for this. Firstly, we only did very few measurements (we could have turned the target by different angles than 180° giving more data). Secondly, we made simplifications in the analytical analysis of the problem which gives rise to systematic errors.

Another important factor is the calibration. We used the same target for calibration and assumed the thickness of gold to be exactly zero. Due to how we measure thickness[9], we still get a non-zero value, but the systematic error of this value is of the same order as the value itself.

Looking at Figure 18, another problem appears when finding the thickness of gold and that is the amount of data in the carbon peaks, which is too low to determine the peaks precisely.

VII. CONCLUSION

The angular dependency of the Rutherford cross section was found to follow the expected expression quite nicely, though with some fluctuations larger than the found uncertainties. A reason for the fluctuations could be that for small angles the carbon and gold peaks were blended together, hence the fitting

---

[9]Measuring the drift of the carbon peak.

of the Gaussians were technically difficult, resulting in larger uncertainties than the calculated uncertainties. The found energy when considering the stopping power is

$$
E_{\mathrm{Au}} = \begin{cases} \left(E_{in} - \frac{T_{\mathrm{Au}}}{2S_{\mathrm{Au}}}\right) K_{\mathrm{Au}}^2 - \frac{T_{\mathrm{Au}}/2S_{\mathrm{Au}}+T_C S_C}{|\cos(\theta)|} , & \theta < \frac{\pi}{2} \\ \left(E_{in} - \frac{T_{\mathrm{Au}}}{2S_{\mathrm{Au}}}\right) K_{\mathrm{Au}}^2 - \frac{T_{\mathrm{Au}}/2S_{\mathrm{Au}}}{|\cos(\theta)|} , & \theta > \frac{\pi}{2} \end{cases} ,
$$
(30)

for gold, and for carbon

$$
E_C = \begin{cases} \left(E_{in} - T_{\mathrm{Au}}S_{\mathrm{Au}} - \frac{T_C}{2S_C}\right) K_C^2 - \frac{T_C/2S_C}{|\cos(\theta)|} , & \theta < \frac{\pi}{2} \\ \left(E_{in} - T_{\mathrm{Au}}S_{\mathrm{Au}} - \frac{T_C}{2S_C}\right) K_C^2 - \frac{T_C/2S_C+T_{\mathrm{Au}}/S_{\mathrm{Au}}}{|\cos(\theta)|} , & \theta > \frac{\pi}{2} \end{cases} .
$$
(31)

The energies of the peaks seen in Figures 13 and 14 shows, that both gold and carbon nicely follow the expected energies, but for carbon there seems to be a systematic error for the small angles making the energy slightly higher than expected. Furthermore the peak due to the stopping power is not visible on the carbon plot, since the data was not possible to acquire due to the structure holding the targets being in the way. For gold the peaks nicely follows the curve with a slightly too high energy for the most angles. The general increase in energy for the peaks is likely partially due to the calibration not taking into account the stopping power.

For the Z-dependence of the Rutherford cross section it was found to be proportional to $Z^{1.8(5)}$ which is

almost Z^2, which we would expect the Z-dependence of the Rutherford cross section to be. The small deviation might be a result of not enough measurements since we have a relatively large uncertainty and a small area of measurements. Having had more heavy nuclei like gold or just some medium heavy nuclei might improve the fit and thus the exponent of the Z-dependence of the Rutherford cross section.

For the thickness of the gold and carbon on the two targets with different theoretical carbon thickness, the found thicknesses of the layers are $t_{\mathrm{Au},1} = 0.05(124) \times 10^3\,\text{Å}$ and $t_{\mathrm{C},1} = 1.40(1) \times 10^3\,\text{Å}$ for the sample with the thickest theoretical carbon layer (sample 1), for which the theoretical values are $t_{\mathrm{Au},1,\mathrm{theo}} = 0.025 \times 10^3\,\text{Å}$ and $t_{\mathrm{C},1,\mathrm{theo}} = 1.500 \times 10^3\,\text{Å}$. For the thin carbon layer (sample 2), the found carbon $t_{\mathrm{Au},2} = -0.05(626) \times 10^3\,\text{Å}$ and

$t_{\mathrm{C},2} = 0.270(2) \times 10^3\,\text{Å}$ for which the theoretical values are $t_{\mathrm{Au},2,\mathrm{theo}} = 0.025 \times 10^3\,\text{Å}$ and $t_{\mathrm{C},2,\mathrm{theo}} = 0.250 \times 10^3\,\text{Å}$. Concerning the thickness of carbon, the found thickness in sample 1 $t_{\mathrm{C},1}$ is fairly consistent with the theoretical thickness $t_{\mathrm{C},1,\mathrm{theo}}$, and the same is true for sample 2. The small deviations may be due to us not being aware of the measurement uncertainties of the "official" measurements. On the other hand, the found thicknesses of gold are worthless due to their uncertainties being several magnitudes larger than the found values $t_{\mathrm{Au},1}$ and $t_{\mathrm{Au},2}$. For this there are several possible explanations: We only went for two measurements of either sample, and we used the calibration to fit away the background, even though the calibration was made from one of the gold-on-carbon samples, and we in the calibration assumed the thickness of the gold to be exactly zero.

[1] W. D. Mackintosh, *Rutherford Scattering*, pp. 403–418. Boston, MA: Springer US, 1974.

[2] D. V. Morgan and E. Bøgh, "On the application of Rutherford scattering and channelling techniques to study semiconductor surfaces," *Surface Science*, vol. 32, pp. 278–286, August 1972.

[3] D. G. Burke and J. C. Tippett, "An application of Rutherford scattering to target thickness measurements," *Nuclear Instruments and Methods*, vol. 63, pp. 353–354, August 1968.

[4] H. Paetz gen. Schieck, *Nuclear reactions: an introduction.* No. volume 882 in Lecture notes in physics, Heidelberg ; New York: Springer, 2014. OCLC: ocn865661723.

[5] J. Coderre, "Radiation interactions with matter: Energy deposition." URL: `https://ocw.mit.edu/courses/nuclear-engineering/22-55j-principles-of-radiation-interactions-fall-2004/lecture-notes/energy_depos_hcp.pdf`. Accessed on October 2$^{\mathrm{nd}}$ 2019.

[6] C. Labaune, C. Baccou, V. Yahia, C. Neuville, and J. Rafelski, "Laser-initiated primary and secondary nuclear reactions in Boron-Nitride," February 2016.